Sensors and Actuators B 255 (2018) 2520–2530

Contents lists available at ScienceDirect

Sensors and Actuators B: Chemical

journal homepage: www.elsevier.com/locate/snb

Research Paper

Efficient fabrication of poly(pyrrole)-nanowires through innovative nanocontact printing, using commercial CD as mold, on flexible thermoplastics substrates: Application for cytokines immunodetection

Alvaro Garcia-Cruz[a,*], Faiza Nessark[b], Michael Lee[a], Nadia Zine[a], Monique Sigaud[a], Raquel Pruna[c], Manuel Lopez[c], Pedro Marote[a], Joan Bausells[d], Nicole Jaffrezic-Renault[a], Abdelhamid Errachid[a,*]

[a] Institut des Sciences Analytiques, Université Claude Bernard Lyon, 5 rue de la Doua, 69100 Villeurbanne, France
[b] Laboratoire d'Electrochimie et Matériaux (LEM), Université de Sétif-1, 19000, Algerie
[c] Departament d'Enginyeries: Electrònica, Universitat de Barcelona, C/Martí i Franquès 1, E-08028 Barcelona, Spain
[d] Centro Nacional de Microelectrónica, Universidad Autónoma de Barcelona, 08193 Bellaterra, Spain

ARTICLE INFO

Article history:
Received 18 April 2017
Received in revised form 30 August 2017
Accepted 8 September 2017
Available online 18 September 2017

Keywords:
Poly(pyrrole)-nanowires
Nanocontact printing
Immunosensor
Electrochemical impedance spectroscopy
Diazonium chemistry

ABSTRACT

Poly(pyrrole)-nanowires (PPy-NWs) were efficiently printed by using nano printing on flexible thermoplastics, and then used to device an impedimetric immunosensor. The present pioneering technology allow to create high sensitive and disponsable immunosensor devised using a low cost and simple fabrication. The innovative nanocontact printing uses a PDMS stamp replicated from a CD mold. The PPyNW printing uses controlled chemical polymerization to print PPy-NWs on poly (ethylene terephthalate) and polyether ether ketone surfaces. Atomic force microscopy analysis of PPyNW revealed a width, height and a separation length of 125 ± 8 nm, 377 ± 5 nm and 172 ± 4 nm, respectively. The PPy-NWs were characterized by scanning electron microscopy (SEM), X-ray photoelectron spectroscopy (XPS) and electrochemical impedance spectroscopy (EIS). The XPS results evidenced the covalent bonding between the thermoplastic surface and the PPyNWs. As a final point, the immunosensor was tested for the quantification of Interleukin 6 recombinant human (IL6, Ag) using EIS. The PPy-NWs were functionalized via diazonium coupling reaction and carbodiimide crosslinker chemistry for the immobilization of Anti-human IL-6 monoclonal antibodies (IL6 mAb's). The developed immunosensor exhibited a sensitivity of 0.013 $(pg/mL)^{-1}$ (linear fitting at $R^2 = 0.99$) and limit of detection (LOD) of 0.36 pg/mL in a linear range of 1–50 pg/mL for Ag IL-6, with a relative standard deviation percentage (RSD%) at 7.6%.

1. Introduction

The new field of nanomedicine integrates nanowire (NW) arrays for the development of novel platforms for various applications such as biosensing [1]. In the recent years, the increasing demand for biosensors has been reported. There is certainly a need to improve their performance and to reduce costs. Nanoscale materials provide an alternative solution, such as NWs that have gained tremendous interest because of their interesting electrical and optical properties and quantum confinement effect, when applied to sensing applications [2]. Also, NWs are very attractive for their integration as a sensing element [3], due to their higher surface area-to-volume ratio. These nanostructures increase sensor sensitivity, offers label-free, direct, and real-time detection at very low concentrations. Devices based on NWs have emerged as one of the most powerful and general platforms for the ultrasensitive direct detection of biological and chemical species, including low concentrations of proteins and viruses [4].

Electrochemical biosensors based on submicron patterned surfaces are of great importance in many fields, especially in medicine for label free detection [5], health care [6], food industry, agriculture, and environmental control [7]. Specially, nanostructured conducting polymers (CPs) are excellent sensing platforms in the design of bio analytical sensors because of their electronic conduc-

* Corresponding authors.
E-mail addresses: alvaro.garcia-cruz@etu.univ-lyon1.fr (A. Garcia-Cruz), abdelhamid.errachid@univ-lyon1.fr (A. Errachid).

http://dx.doi.org/10.1016/j.snb.2017.09.057
0925-4005/

tivity, low energy optical transitions, biocompatibility, and room temperature operation [8]. Among them, polypyrrole (PPy) is one of the most extensively used conducting polymers because of a number of properties such as redox activity, rapid electron transfer, and ability to link a variety of biomolecules to pyrrole groups by chemical treatment [9]. However, the use of conducting polymer nanowires (CP-NWs) for biosensing applications is limited due to their incompatibility with traditional micro-fabrication processes such as lithography and focused ion beam due to its potential thermal damage during these processes. Numerous methods of assembling CP-NWs to fabricate biosensors have been reported, for e.g., electro spinning, electro polymerization etc [10,11]. Generally, PPy-NWs are largely synthesized by electrochemical polymerization and applied to biosensors [12,13]. Commonly, PPy-NW are synthetized by electropolymerization using a template [14] and then used to fabricate chemiresistive biosensors [15]. Despite the increasing number of nano-engineered technologies and materials, the PPy-NW fabrication require several steps, different time consuming techniques, which are expensive and limited.

New biosensor technologies integrate PPy-NWs functionalized with biomarkers and antibodies for healthcare diagnosis [16,17]. Recent advances in proteomics make in evidence new biomarkers (for e.g. cytokines), resulting in promising tools to diagnose cancer [18]. These studies intended to detect the inflammatory cytokines that might augment in serum as a diagnostic marker for cancer. Additionally, cytokines are very useful for clinical evaluation of patients [19]. Typical biomarker diagnostics is based on the detection of cytokines levels (interferon-γ (IFN-γ)), tumor necrosis factor-α (TNF-α), tumor growth factor-β (TGF- β), and interleukins (IL) (IL-1β, IL-2, IL-4, IL-5, IL-6, IL-8, IL-10, or IL-13) in several types of cancer such as bladder [20], pancreas [21], prostate [22], lungs [23], and thyroid [24] cancer. These cancer biomarkers are usually detected by common immunoassay techniques. The gold standard is enzyme-linked immunosorbent assays (ELISAs) [25–27].

Electrochemical immuno-sensors are promising alternative to ELISA tests that are vastly used for cancer and clinical diagnosis [28,29]. Immuno electrochemical sensors devices are based on electrical measurements that employ the specific bio molecular recognition of the antibody-antigen (Ab-Ag) complex, for a desired biomarker of interest. An electrochemical biosensor provides quantitative values for the analyte of interest at reduced costs and analysis time. However, despite the wide spectrum of possibilities, there are still some limitations to improve. Unfortunately, the current fabrication technology of immunosensor requires several steps and time consuming process such as photolithography and expensive semiconductive materials. Currently those techniques are not suitable for large scale production and also difficult to employ for common medical applications as diagnostics. Next generation sensor platforms will require important improvements in fabrication, reproducibility, and flexibility, however especially in sensitivity and specificity [30] in order to meet the future needs in medicine prevention of cancer and chronic diseases.

Here, in this work, we overcame these difficulties by introducing an efficient, low-cost, and easy Poly(pyrrole) nanowires (PPy-NW) printing process. The conducting PPy-NW were printed using the nanocontact printing and controlled chemical polymerization (nCP-CCP) technique on flexible thermoplastic films (poly (ethylene terephthalate) (PETE) and Polyether ether ketone (PEEK)). PPy-NWs were functionalized via diazonium coupling reaction and carbodiimide crosslinker chemistry for the immobilization of specific antibodies (anti-human IL-6 monoclonal antibodies, mAbs). The modified PPy-NW was tested as an impedimetric immunosensors for the detection of human IL-6. The innovative fabrication technology presented herein, bring the disposable immunosensors high sensitive, accessible and easy to produce with inexpensive.

The diazonium chemistry [31,32] has been used to tailor functionalities in a large variety of materials [33], for e.g., carbon (single-walled carbon nanotubes (SWCNTs), glass carbon, diamond, etc), semiconductors (silicon), metals (gold and platinum), and PPy [34–37]. The fabrication of electrochemical immunosensors [38,70] based on the covalent immobilization of linkers via diazotization coupling reaction have been successfully reported before in different materials, for e.g., screen printed carbon electrodes (SPCEs), glassy carbon electrodes (GCEs), graphene modified electrodes, gold electrodes, gold nanoparticles, and diamond electrodes [39–44].

Here, we present the fabrication of an impedimetric immunosensor based on PPy-NWs functionalized via diazonium coupling reaction for the immobilization of specific antibodies (anti-human IL-6 mAbs). At first, 4-phenylacetic acid film was grafted by electrochemical reduction of the diazonium salt (from the 4-aminophenylacetic acid, (4APAC)), followed by terminal carboxylic group activation by *N*-hydroxysuccinimide (NHS) and *N*-(3-dimethylaminopropyle)-*N*-ethyle-carbodiimide hydrochloride (EDC). Subsequently, the carboxyl group activation of 4-phenylacetic acid was conjugated to the terminal amine groups from the antibodies through amide bond formation. After antibodies immobilization, detection of the respective antigen was achieved by using electrochemical impedance spectroscopy (EIS). The PPy-NW functionalization was evaluated using electrochemical methods (cyclic voltammetry (CV)) and EIS, as well as by scanning electron microscopy (SEM).

2. Experimental section

2.1. Chemicals

2.1.1. Polymers

PDMS (Sylgard 184) was purchased from Dow Corning, France. The applied thermoplastic films were PEEK (HN, 125 μm, DuPont) and PETE (125 μm, Goodfellow).

2.1.2. Chemicals and reagents

11-(triethoxysilyl)undecanal (TESUD) was purchased from Gelest, USA. *N*-(3-trimethoxysilyl-propyl) pyrrole (Py-silane) was purchased from ABCR GmbH & Co. KG, Germany. 3-Aminopropyltriethoxysilane (APTES), Sulfuric acid (H_2SO_4, 30 wt.% in H_2O), phosphate buffered saline (PBS) buffer, sodium dodecyl sulphate (SDS), iron (III) chloride, Pyrrole, 1-Ethyl-3-(3-dimethylaminopropyl) carbodiimide hydrochloride (EDC), *N*-hydroxysuccinimide (NHS) were purchased from Sigma Aldrich, France. Hydrogen peroxide (H_2O_2) (35% wt.) and potassium hydroxide (KOH) were obtained from Acros Organics, France.

2.1.3. Biological reagents

Preparations were performed following the recommendation from the supplier (R&D systems, USA) [45].

The *E. coli*-derived recombinant human IL-1 beta/IL-1F2 (IL-1) was reconstituted at 25 μg/mL in sterile PBS. The corresponding E. coli-derived recombinant human IL-1β/IL-1F2 antibody (IL-1 rh antibody) was reconstituted at 0.5 mg/mL in sterile PBS.

The *E. coli*-derived recombinant human IL-6 (IL-6) was reconstituted at 100 μg/mL in sterile PBS. The respective E. coli-derived recombinant human IL 6 monoclonal antibody (IL-6 rh antibody) was reconstituted at 0.5 mg/mL in PBS.

The *E. coli*-derived recombinant human IL-8 (IL-8) was reconstituted at 100 μg/mL in sterile PBS. The corresponding E. coli-derived recombinant human CXCL8/IL 8 antibody (IL-8 rh antibody) was reconstituted at 0.5 mg/mL in sterile PBS.

The Sf 21-derived recombinant human IL-10 (IL-10) was reconstitution at 0.5 mg/mL in PBS. The respective Sf 21-derived

recombinant Human IL-10 (IL-10 rh antibody), mouse IgG1 class. Monoclonal antibody was reconstituted at 0.5 mg/mL in PBS.

2.2. Methods and techniques

Microcontact Printer: Semi-automatic Micro-Contact-Printing System μ-CP 3.0 from GeSiM Gesellschaft fuer Silizium-Mikrosysteme mbH, Germany.

2.2.1. EIS measurements

Experiments were acomplished in a miniaturized electrochemical Teflon cell and the PPy electrode was set as the working electrode (WE). Perpendicular to that, a platinum counter electrode (CE) and a silver (Ag/AgCl) reference electrode (RE) were used to complete the three electrode system. The experiments were carried out in a freshly prepared 5 mM PBS buffer solution at pH 7.4 as electrolyte. The EIS technique was performed in a Potentiostat EC-lab VMP3 instruments version 9.9 and controlled and modelled using EC-Lab software V10.39, 2014 by Bio-Logic-Science Instruments, France. The data impedance was normalized with the fitting software. For the Z-fit, the Nyquist plots were observed with randomize + simplex method, with randomize stopped on 10,000 iterations and the fit stopped on 5000 iterations respectively. The applied conditions (potential, sinus amplitude, and frequency) were at −0.1 V, 25 mV, 100 kHz to 100 MHz, respectively (35 s/scans). The fitting was dependent on the form of the semi-circle curves obtained in the Nyquist plot. The selection of the equivalent circuit was dependent upon the interfaces of the Nyquist plot to produce the smallest error that was expressed in the standard deviation (X^2).

2.2.2. Microscopy

All *optical microscope* images were made with an Axio Vision (*Carl Zeiss Microscopy*, France). The stereo microscopy images were obtained with an EZ4D (*Leica Microsystems*, France).

Scanning electron microscope (SEM) images were obtained with a *Hitachi* SEM S800, France.

Atomic force microscopy (**AFM**) images were obtained with a Nano observer (*CSI Company*). The maximum and minimum resolution of the AFM was 110 μm^2 and 5 μm^2, respectively. An Ultrasharp Silicon Cantilever CSC17/Ti-Pt/15 MikroMasch tip was employed. The silicon chip thickness of the silicon cantilever (SC17) was 0.4 mm and less than 35 nm for the curvature radius. Tip characteristics were: height of 15–20 μm, full tip cone angles less than 30°, tip and both sides of the cantilever were consecutively coated by continuous films of Ti (15 nm, 1 st layer) and Pt (10 nm, 2nd layer). Cantilever Specifications: typical length at 460 ± 5 μm, width at 50 ± 3 μm, and thickness of 2 μm. The resonant frequency was 304.14 kHz and an amplitude of 1.756 V. The Force constant was 0.15 N/m (0.05–0.30). Measurements were taken in contact mode with a speed of 0.75 line/s and 1024 resolution.

2.3. Activation process

The effectiveness of NaOH (aq) treatment to the modified PEEK [46,47] and PETE [48–50] was stablished previously. Here, the thermoplastic substrates were cleaned by sonication and rinsed, first with propanol and then with distilled water. PETE and PEEK substrates were treated with ultraviolet irradiation (320 nm, 10 min) and then activated in KOH (3 M) solution for 5 min [51]. This treatment generated hydroxyl groups onto the surface. Afterwards, the substrates were thoroughly rinsed with distilled water and dried with nitrogen. The activated polymers were characterized after activation using SEM as shown in Fig. S1. The PPyNW are covalently bonded to the activated thermoplastic surface via silane chemistry [52,53].

2.4. Master mold preparation

A standard CD contains a nano-patterned plastic layer, this layer consists of wire arrays with a typical depth and width of ∼180 nm and ∼800 nm, respectively [54]. The AFM characterization of the CD mold is shown in Fig. S2. The nanostructured master mold was obtained from a commercially compact disk (CD, 700MB, 52X, Maxell). The samples (1 cm^2) were first ultrasonically cleaned in acetone for 5 min. The nanopatterned plastic layer was obtained by treating the sample with nitric acid (60% solution, 5 min), then rinsed in Milli-Q water and ethanol, and finally dried under nitrogen. The nanopatterned plastic layer was used as the mold, and replicated in PDMS.

2.5. PDMS stamp fabrication

The nanostructured PDMS stamp was obtained by replica molding using the nanostructured plastic part of a commercial CD as a master mold. Stamps for nCP were fabricated from elastomeric PDMS by mixing a 10:1 ratio (w/w) of the pre-polymer and the cross-linker following the recommendations of the supplier [55]. The mixture was first degassed, poured on the nanopatterned plastic surface, and cured at 80 °C for 1 h. The CD nanopatterned arrays were transferred to the PDMS surface by casting. After curing, the nanopatterned PDMS stamps were fixed to a semi-automated microcontact printer. The nano patterned PDMS stamps produce a high quality printing of PPy-NWs and this printing mode has been used before within our group for nCP of thiols [56–58]. The AFM imaging for the PDMS stamp is shown in Fig. S2.

2.6. PPy-NW printing process

We have developed a nCP of PPyNW on thermoplastics substrates using a PDMS stamp replicated from a CD mold. The thermoplastic surfaces were previously activated. Subsequently, the nanostructured PDMS stamp was inked with a monomer, catalyst, and surfactant (0.42 M Py-silane, 0.01 M SDS and 1 M $FeCl_3$). Before printing, the μ-CP printer was configured with a pressure of 128.5–129 KPa, printing level of 25.8 mm and 4 μL ink per 1 cm^2. Afterwards, the surfaces were brought into conformal contact and the printed surface was then heated at 45 °C. The inking time was 20 s and printing time of 15 min at 45 °C. The process occurred in a single step. The PPyNW were characterized using AFM and SEM (FigS and FigS).

2.7. Preparation of diazonium salts

A 4.2 mM solution of 4-aminophenylacetic acid (4APAC) was prepared in 1 mL of an aqueous HCl solution (1 M)/ethanol 50:50 (v/v), named solution 1, (S_1). A second solution (S_2) was prepared containing 89 mM of sodium nitrite in 1 mL of a water/ethanol mixture (50:50). For the diazotisation, 44 μL from S_2 was mixed with 956 μL of S_1 and then stirred in ice (−2 °C, 5 min). Successively, the mixture S_1-S_2 is diluted in 20 mL of a solution containing HCl (0.1 M)/ethanol (50/50) aqueous solution (stirring at 0 °C) to obtain a 0.19 mM solution (S_3) of the diazonium salt [59]. The solution (S3) was placed into the electrochemical cell for the electro reduction. Electro reduction of the aryldiazonium salt on the PPy electrode is performed by cyclic voltametry (CV) between a potential of 0.1–1.3 V at 50 mV/s (see, Fig. 4).

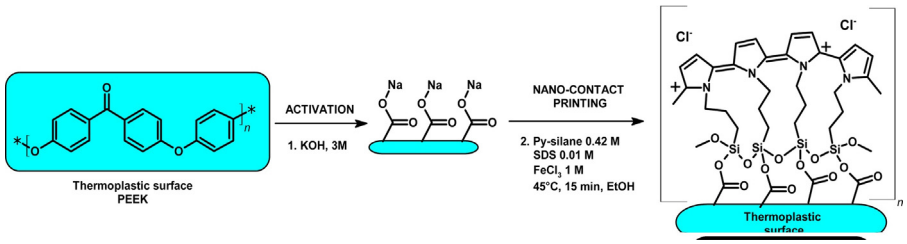

Fig. 1. (1) Activation process and (2) PPy-NW printing by nCP-CCP to finally produce the chemical structure of PPy oxidized.

3. Results and discussion

3.1. Thermoplastic polymers activation

PEEK and PETE surface was characterized using SEM as shown in Fig. S1a/c (section 1, Supporting Information). Here, we observed that PEEK and PETE behaved different to the activation process due their chemical structure coffering resistance to the KOH treatment. Both thermoplastic surfaces after activation became more hydrophilic and roughness was increased. The PETE and PEEK during the activation process produced carboxylic groups by hydrolysis, as shown schematically in Fig. 1.

3.2. PPy-NW electrode fabrication

Conductive PPy-NWs were printed on the thermoplastic substrates by using nCP-CCP. A commercial CD was replicated to produce a nano patterned PDMS stamps, and then employed to print PPy-NWs. The CD mold and PDMS as well as the PPyNW printed on thermoplastic surfaces wer characterized using SEM (Fig. S1) and AFM (Fig. S2). Additionally, an analysis of the nanocontact printing patterm transfer is presented in supporting information Section 2. Further discussion regarding the reproducibility and reliability of the PPyNW fabrication method can be found in this section.

The printed PPy-NWs were fabricated at 747 ± 12.2 nm (width), 114 ± 8 nm (height) and a separation length of 573 ± 13.4 nm, as shown in Fig. S1 b/d. The ink formulation was composed of *N*-(3-trimethoxysilypropyl) pyrrole monomer (Py-silane, 0.42 M), sodium dodecyl sulphate as structural agent (SDS, 0.01 M) and Iron(III) chloride as catalyst ($FeCl_3$, 1 M) in ethanol solvent. The molar ratio catalyst to monomer was set at 7:3. The nCP-CCP was performed at 45 °C for 15 min. The nCP-CCP technique enabled chemical bonding of the PPy to the thermoplastic surface. The printed PPy-NW on thermoplastic films were used as electrodes. The fabrication process is shown schematically in Fig. 1.

3.3. PPy-NW characterization by X-ray photoelectron spectroscopy (XPS)

PEEK and PETE thermoplastic films were studied before and after PPy printing using X-ray Photoelectron Spectroscopy (XPS). The activated thermoplastic surfaces show the characteristic signals of C 1s and O1s species. Subsequently to the PPy printing, the relative increment on C1s and O1s species were detected, besides new species were present, for e.g., N1s, Si 2p, Fe $2p^3$ and Cl 2p, that probed PPy silane was deposited on the thermoplastic surfaces. Additionally, the presence of Cl 2p and Fe 2p revealed that the PPy was oxidized [60]. After XPS spectra normalization, atomic relative percentage was calculated for the elemental analysis from each sample.

3.3.1. PETE characteristics

The PETE polymer presents typical signals of C1s and O1s species [61] (Fig. S3). XPS high-resolution spectra from PETE activated surface displays distinctive peaks located at 284, 285.5, and 288.4 eV attributed to the C—C/C—H, C—O/C—O—C, O—C=O/C=O signals, respectively (Fig. 3a).

After PPy printing, the N1s signal appeared (from the PPy), the C1s signal decreased and the O1s increased. The O1s, Si 2s, and Si 2p species were increased due to the presence of silane Si—O groups on the PPy-silane. These characteristic signals demonstrated that PPy-silane was covalently bonded to PETE surface. In addition, the presence of Cl 2p and Fe 2p corresponded to the oxidant of $FeCl_3$ which reveals that the PPy-NW film was in its oxidized state [62]. The collection of XPS spectra from PETE activated and modified with PPy-NW is shown in Fig. S3 and Table S2 (Section 3, Supporting Information). The apparition of the N1s, Si 2p, Cl 2p, and Fe $2p^3$, and also the oxygen content in the sample increased proving that PPy was successfully deposited on the surface. XPS high-resolution demonstrate the presence of PPy, distinctive peaks were observed at 285.5 and 287.8 eV corresponded to the C—O/C—O—C and O—C=O/C=O signals, respectively. This surface modification caused decrement on the carboxyl groups (C—O, C=O) as shown in Fig. S4.

3.3.2. PEEK film characterization

The activated PEEK polymer presents specific signals of C1s and O1s species [63–65] (Fig. S5 and Table S3, Section 3, Supporting Information). After PPy-NW printing, the N1s signal appeared (from the PPy), the oxygen increased. The O1s, Si 2s and Si 2p species increased due to the presence of the siloxane polymer part (Si—O groups) on the PPy-silane. These signals provide evidence that PPy-silane was deposited on the PEEK thermoplastic surface. Furthermore, the presence of Cl 2p and Fe 2p proved that the PPy-NW film was doped [66].

XPS high-resolution analysis (Fig. S5) for activated PEEK surface exhibited distinctive peaks at 284.3, 285.4 and 291.4 eV attributed which corresponded to the C—C/C—H, C—O/C—O—C and the $\pi - \pi*$ satellite band, respectively (Fig. S5a). Subsequently, the PEEK modified surface with PPy-NW presented C—C/C—H, C—O/C—O—C, O—C=O/C=O signals at 284.4, 285.3 and 287.6 eV respectively (Fig. S5b). The deposition of the PPy-NW caused the decrement of carboxyl groups (C—O, C=O) due to the presence of the silane bonding.

3.4. Electrochemical studies

3.4.1. PPy characterization by electrochemical impedance spectroscopy (EIS)

The electrical properties of the PPy films were studied by EIS. The obtained EIS data was plotted as a Nyquist plot model with a corresponding equivalent circuit [67]. The resulting EIS curves were fitted and the component values were extracted using equivalent circuit chosen according to the interfaces obtained in the Nyquist plot of the semicircles. The Nyquist plot represented the imaginary impedance −Im(Z) against the real impedance Re(Z). Here,

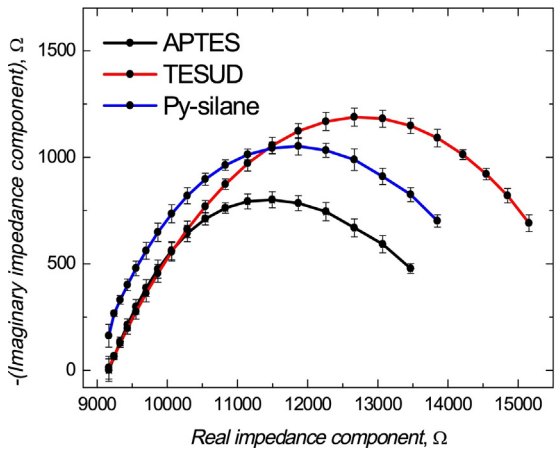

Fig. 2. Nyquist plot of PPy films prepared with: a) APTES and Py-silane, b) TESUD, and c) Py-silane. The experiments were carried out at a frequency range between 100 kHz and 100 MHz and a drop potential of (E = −0.138 V/(Ag/AgCl).

we applied the equivalent circuit ($R_1 + Q_2/R_2$) to calculate the best fit of the data. The equivalent circuit consistent of capacitive and resistive components, where: R_1 represented the resistance due to the electrolyte solution. R_2 is the resistance of the WE (PPy matrix) and the Q is the constant phase element, related to the capacitive phenomena.

3.4.2. Influence of the silane linker into the PPy properties

We studied the electrical properties and topography changes induced by the silane linker into PPy chemically polymerized into the PEEK surfaces. Silane linker was chemically bonded on PEEK surface (previously activated). Silane linker was deposited by drop coating and then cured at 80 °C for 1 h. PPy chain was chemically polymerized on the top of the silane linker layer as shown in Fig. S6 (Section 4, Supporting Information). We studied three different silane linkers for PPy deposition, 11-(triethoxysilyl)undecanal (TESUD), *N*-(3-trimethoxysilyl-propyl) pyrrole (Py-silane) and 3-Aminopropyltriethoxysilane (APTES). We observed that each silane assembled differently due to their affinity to the activated thermoplastic surface, resulting in different PPy properties. More detailed experimental information concerning the silanes linkers deposition and PPy chemical polymerization is shown in Fig. S6.

Electrical properties and structuration of the PPy film was affected by the silane linkers. PPy films were imaged and measured using SEM and EIS, respectively. The resulting PPy films were firstly studied by EIS and represented in a Nyquist plot shown in Fig. 2. Apparently, the PPy conductivity and adherence to the thermoplastic surface was improve when using APTES. The silane linkers influenced the PPy film conductivity in this order TESUD < Py-silane < APTES (Fig. 2). Furthermore, SEM imaging demonstrate the surface modification for each step, firtly the silane linker deposition on PEEK, subsequentlyto the PPy deposition and then electrodeposition of diazonium salts on the PPy surface (PPyPAC).

SEM imaging for the silane deposition on PEEK is shown in Fig. 3a/d/g. Py-silane produced a rough surface with grains (Fig. 3a). APTES deposition resulted in the formation of a crystaline web (Fig. 3d). TESUD deposition resulted in flakes formation (Fig. 3g). Succeeding to the silane linker deposition, PPy was chemically deposited on the top as shown in Fig. 3b/e/h. The PPy grew using Py-silane resulted in a rough surface decorated with grains and crystals (Fig. 3b). The PPy produced using APTES presented a filament assembling. TESUD linker produced multilayer structures of PPy covered with grains (Fig. 3h). Finally, the PPy film was modified by the electroreduction of diazonium salts (Fig. 3c/f/i). The electrodeposition modified the PPy topography, resulting in a highly porous assembling. In conclusion, the APTES linker after electromodification resulted enhanced electrical properties and presented best adherence.

3.4.3. Electroreduction of aryldiazonium salts on PPy electrodes

PPy-NWs were functionalized via electro reduction of diazonium salts. Diazotization of 4-amino-phenyl acetic acid, subsequently to their electro reduction resulted in electrodeposition of 4-phenyl acetic acid layer on PPyNW (see, Section 2.7). Electro-reduction was carryout using CV performed in a potential range between 0.1 and −1.3 V/(Ag/AgCl) and a scan rate of 50 mV/s, 15 cycles (until saturation) in PBS buffer. The first cycle presented a reduction wave, for the diazonium, proving successful electrodeposition of 4-phenyl acetic acid layer at the PPy-NW electrode surface (Fig. 4A). Also a slightly reduction peak was observed at −0.5 V/(Ag/AgCl) attributed to the reduction of hypo phosphorous acid H_3PO_2 from the buffer solution. The second reduction wave, observed at −0.9 V/(Ag/AgCl) was higher and more defined. This second wave corresponded to the reduction of the cation aryl diazonium at the polymer surface, by the reduction of nitrogen and the phenyl acetic acid radical deposition on the PPy surface. The reduction of the cation aryl diazonium salt is typically observed by other authors at −0.75 V/(Ag/AgCl) on graphite microarrays [68], at −1.1 V/(Ag/AgCl) in the case of gold [69] and graphite electrodes [69], and in reduced PTFE at −1.4/(Ag/AgCl) [71]. The diazonium species reduction is an irreversible cathodic process. Afterwards, the electrode surface during cycling was saturated due to the isolating organic film deposition on the PPy-NW surface. This provided the formation of phenyl acetic acid layers. Contrary to our experience, diazonium salt reduction into carbon electrodes is observed from the first cycle and there are not saturation phenomena during cycling. During the reduction process, the organic film growth into the PPy surface resulted in an increment of surface area of the electrode and, therefore, it became rougher and less conductive [72,73].

The previously reported electro reduction of diazonium salts on PPy film [4] showed in the first voltammetric cycle, a reduction peak at +0.16 V due to reduction of the diazonium salt. Peaks corresponding to reduction and oxidation of the polymer were observed at −0.25 V at −0.15 V, respectively. In the next cycle, only the reduction and oxidation peaks of the polymer can be observed. The redox potentials of the PPy films stabilized at about−0.4 V for reduction and at about 0.3 V for oxidation. These differences are related to the PPy-NW electrochemical properties, which differs from the PPy film prepared electrochemically, since our printing technology is based in a chemical polymerization. On the other hand, compared with the carbon electrode [3–6], the saturation was obtained from the first cycle. Furthermore, a shift on the reduction potential from the aryl diazonium compound was located in more positive values. In our case, we did not observe any positive sweep potential. This confirmed that the diazonium did not oxidize and the surface grafting process was irreversible. The coverage rate of the phenyl acetic acid deposited film was calculated at Θ = 76.54%.

3.4.4. Electrochemical characterization of the PPy modified electrodes (PPyPAC)

The electrochemical performance of PPyPAC electrodes was studied firstly by CV. The voltammograms from the original PPy and modified PPyPAC electrodes were compared as shown in Fig. 4**B**. The cyclic voltammograms were recorded over a range of potential between −0.85 and 0.1 V/(Ag/AgCl) and a scanning rate of 50 mV/s in PBS buffer solution (pH 7.4, surface electrode area, Ø = 50.3 mm^2). The voltammogram from the PPy electrode (Fig. 4**Ba**) showed (cathodic potentials) a weak PPy oxidation wave observed at 0 V/(Ag/AgCl), and (anodic potentials) displayed two weak peaks at − 0.2 V and −0.5 V/(Ag/AgCl), respectively. These

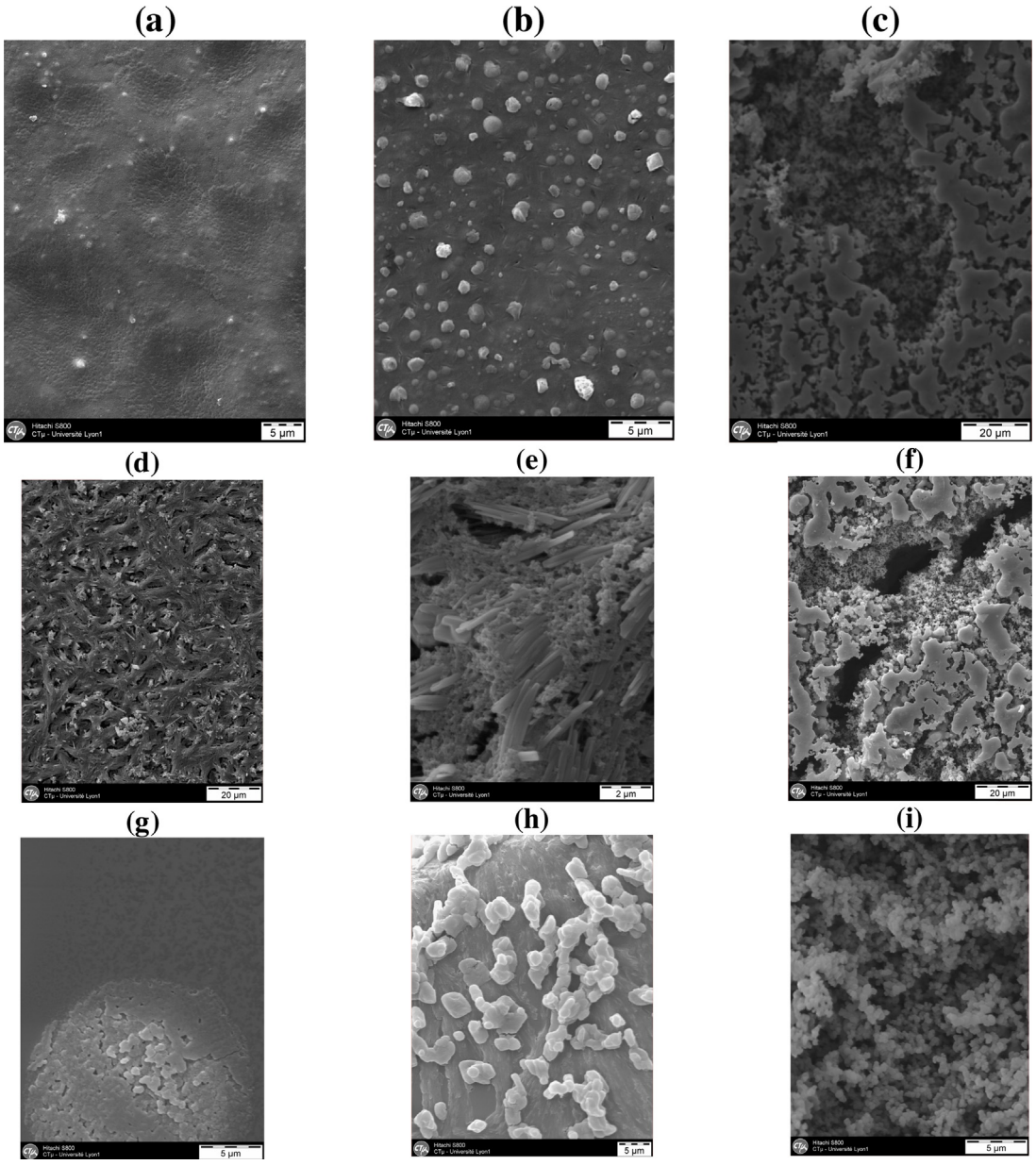

Fig. 3. SEM images of silane linker deposition (a, d, c) on PETE substrates. Later on, PPy growth (d, e, h), and after electro reduction of diazonium salts on the PPy surface (c, f, i). In (a) Py-silane deposition on PETE (5 µm scale bar). (b) PPy obtained using Py-silane (scale 5 µm). (c) PPy modified by electro reduction of diazonium salts (scale 20 µm). (d) APTES grafted on PETE. (e) PPy on APTES layer. (f) The electro modified PPy film with diazonium salts. The (g) TESUD silane deposition on PETE (scale 5 µm). (h) PPy prepared on TESUD. (i) The PPyPAC modified surface.

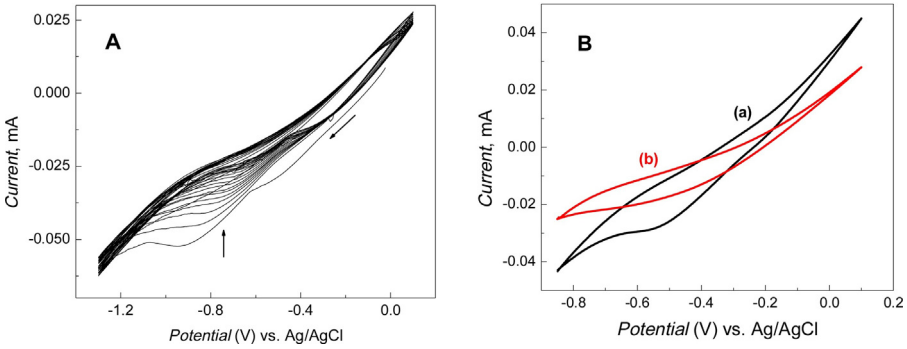

Fig. 4. (A) Successive voltammograms from the aryldiazonium (0.19 mM) electro reduction on PPy* electrode over a potential range between 0.1 and −1.3 V/(Ag/AgCl) at 50 mV/s (*conductive PPy-NW printed on PETE). (B) Cyclic voltammograms from (a) PPy electrode and in (b) after modification with PPyPAC. Experiments were recorded between −0.85 and 0.1 V/(Ag/AgCl) at 50 mV/s (PBS, pH 7.4, Ø = 50.3 mm2).

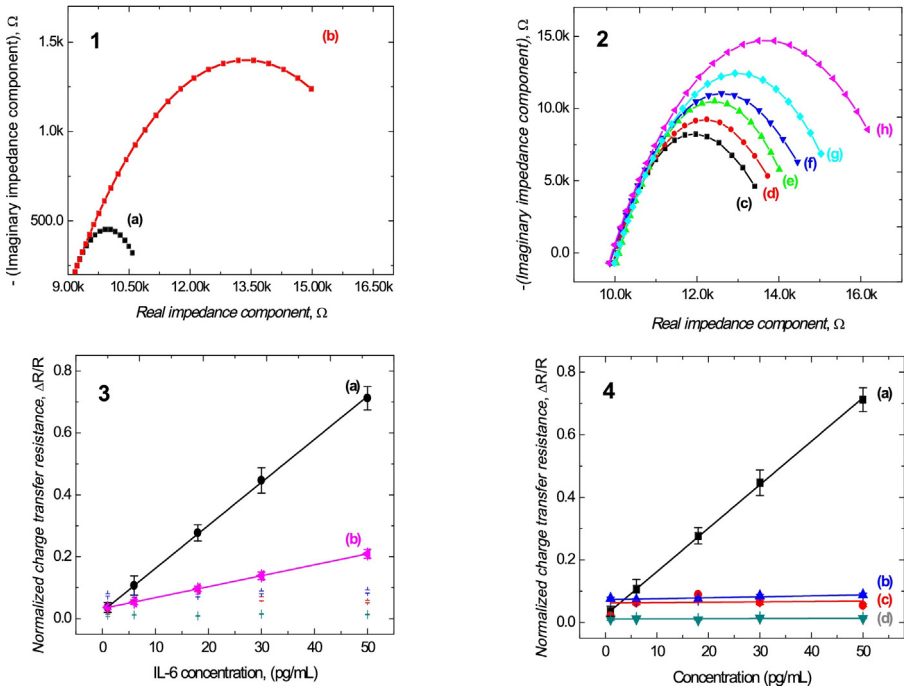

Fig. 5. Nyquist plot 1, shows the (a) PPy electrode and the(b) PPyPAC electrode. Nyquist plot 2, present in (c) the PPyPAC modified with antibody IL6. Afterwards, detection of the corresponding IL6 antigen: (d) 1 pg/mL (e) 6 pg/mL, (f) 18 pg/mL (g) 30 pg/mL and (h) 50 pg/mL. In 3, comparison of the EIS determination of antigen IL-6 using (a) PPyNW and (b) bulk PPy. In 4, response of the immunosensor selective to IL-6 for (a) IL-6, (b) IL-8, (c)IL-10 and (d) IL-1. The immuno sensor presented a LOD of 0.36 pg/mL. The analysis was performed in PBS solution (pH 7.4) at r.t., over a range of frequency between 100 KHz and 100 MHz at a drop potential of (E = −0.138 V/(Ag/AgCl).

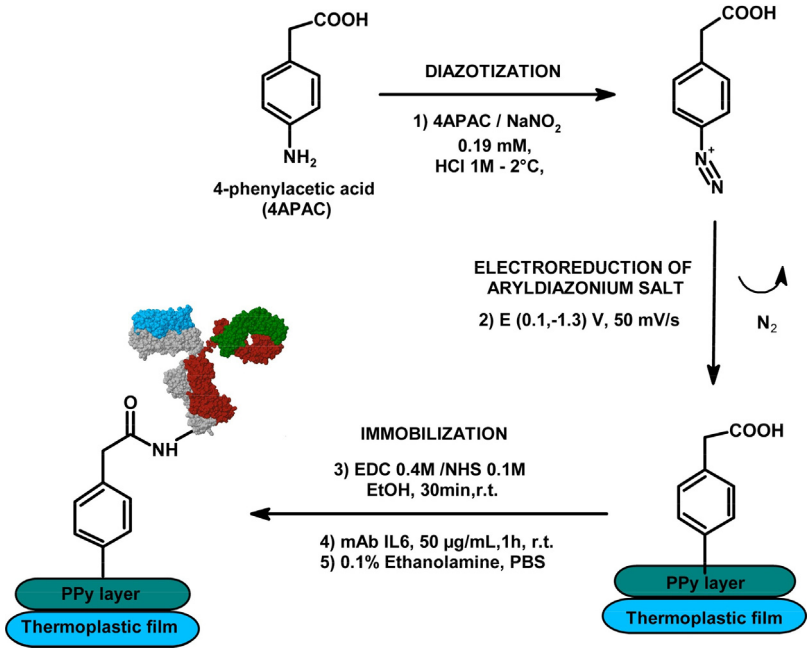

Fig. 6. The immuno sensor is fabricated by modifying the PPy-NW via electro reduction of a 4-phenylacetic diazonium salt (PPyPAC layer). IL6-mAb are immobilized using EDC/NHS chemistry.

corresponded to the reduction of the PPy film and the hypo phosphorous acid H_3PO_2 from the electrolyte solution. The last signal was also observed during the electro reduction of the aryl diazonium salt into the PPy electrode. The voltammogram in (Fig. 4**Bb**) from the modified electrode PPyPAC, showed a complete disappearance of oxidation and reduction waves from PPy film. This evidenced the electro deposition of the isolating phenyl acetic acid layer. This method on PPy film surface offers the advantages of preserving the electrical conductivity and mechanical strength of the film.

3.4.5. Electrode characterization and antigen interleukin 6 detection by EIS

EIS measurements were performed and the Nyquist plots from the PPyPAC modified electrode was compared against the original PPy electrode (Fig. 5Aa). EIS was carried out in PBS (pH 7.4) at a drop potential of (E = −0.138 V/(Ag/AgCl) and at a frequency range

Table 1
Immunosensors comparison of their analytical parameters

Cytokine	Concentration range (pg/mL)	LOD (pg/mL)	Transducing technique	Ref
IL-6	1×10^{-5}–0.1	1×10^{-5}	EIS	[78]
IL-6	0.005–0.05	0.005	Amperometry	[79]
IL-6	1–50	0.013	EIS	This work
IL-6	0.02–20	0.02	EIS	[80]
IL-4	50–70000	0.02	Chemiluminescent	[81]
IL-8	0.1–1000	0.03	EIS	[82]
IL-1, IL-6	0.015–11	0.01–0.04	Amperometry	[83]
IL-6	$0.1–1 \times 10^5$	0.059	LSV	[84]
IL-6	$0.5–1 \times 10^4$	0.1	DPSV	[85]
IL-10	0.1–20	0.1	EIS	[86]
IL-6	1–40	0.3	Amperometry	[87]
IL-1	0.5–100	0.38	Amperometry	[88]
IL-6	$1.0–1 \times 10^4$	0.38	Amperometry	[89]
IL-6	1.75–500	0.39	Amperometry	[90]
IL-6	0–400	0.41	Amperometry	[91]
IL-6	2–20,000	1.0	SWV	[92]
IL-6	4.0–800	1.0	Amperometry	[93]
IL-6	1.0–100	1.37	FET	[94]
IL-6	$5–5 \times 10^4$	2	SWV	[95]
IL-12	$0–1 \times 10^4$	4	EIS	[96]
IL-6	4.7–300	4.7	FET	[97]
IL-6	20–400	20	Amperometry	[98]
IL-8	62.5–2000	72.4	Amperometric	[99]
IL-8	$0.9–9 \times 10^5$	90	EIS	[100]
IL-6	$1 \times 10^3–1 \times 10^5$	1000	Amperometry	[101]
IL-10	1.0–10	–	EIS	[102]
IL-1, IL-6, IL-10	1.0–15	–	EIS	[103]

between 100 KHz and 100 mHz. The resulting PPyPAC electrode after reduction of the diazotization process showed more capacitive behaviour than the PPy polymer alone. The isolating deposited on PPy surface was evidenced by the increase of the charge transfer resistance (Rct). (Fig. 5Ab). After PPy film was modified with diazonium salts into PPyPAC, the antibody immobilization was performed via carbodiimide chemistry.

The carboxyl groups of 4-phenylacetic acid film (PPyPAC modified electrodes) was activated by EDC/NHS (0.4 M/0.1 M in ethanol, 30 min at r.t.) and then conjugated to terminal amine group from the antibodies through amide bond formation. Subsequently, PPyPAC electrodes were functionalized with anti-IL-6 mAb's (50 μg/mL in PBS for 1 h). After incubation, 0.1% ethanolamine in PBS was added to deactivate the unreactive sites (30 min). The comparison between PPyPAC electrode before and after antibody immobilization (PPy-Ab) is shown in (Fig. 5Bc). The recognition of the respective antigen human IL6 was determined using EIS. For that purpose, a standard calibration curve was prepared measuring IL6 solutions with a concentration rage of 1 pg/mL to 50 pg/mL (incubation 30 min at r.t. in PBS), (Fig. 5Bd–h). The curve obtained after the immobilization of anti-IL6 mAb became less capacitive with respect to the PPyPAC curve due to the charge transfer properties conferring to the surface (Fig. 5B). We found that during IL6 detection, the Nyquist plot presented in the high frequencies similar angle phase of 45° (Fig. 5B).

The immobilization process is schematically presented in Fig. 6. Determination occurred only at the low frequencies. This is accompanied by the increase of the polarization resistance due to the capacitive layer phenomenon owing to the detection on the PPy-Ab electrode surface. After incubation with different increasing concentrations, the plot clearly shows that Rct increases with the increased concentration of IL-6 antigen. This indicates that the PPy-IL6-mAb electrode was successfully operational as a immunosensor. From the Nyquist plot antigen IL6 detection (1–50 pg/mL) a calibration curve (Fig. 5C) was obtained ploting the normalized Rct measured ($\Delta R = [Rct_{Detection} - Rct_{Antibody}]/Rct_{Antibody}$) against the IL-6 concentration [74]. The immunosensor presented a sensitivity of 0.013 $(pg/mL)^{-1}$ (linear fitting at $R^2 = 0.99$) and a limit of detection (LOD) of 0.36 pg/mL. The reproducibility of the Immunosensor was calculated with a relative standard deviation percentage (RSD%) at 7.6%.

In addition, the PPy bulk film presented a sensitivity 0.004 $(pg/mL)^{-1}$ and LOD of 3.3, ($R^2 = 0.98$). These results revealed that PPyNW are 3.2 times higher sensitive when compared to the PPy bulk, proving that the high sensitivity of the PPyNWs.

The immunosensors is highly selective to IL-6, as shown in **Fig**. When the immunosensors was exposed to a different IL interferent (IL-1, IL-8 and IL-10) the response was three orders of magnitude lower and nonlinear response was obtained.

3.4.6. Performance PPyNW base immnunosensor

Previous reported electrochemical cytokine interleukin immunosensors have shown the possibility of determination at sub nano scale concentration. Nevertheless, the sensor preparation methods still tedious, time consuming, costly materials and techniques for surface modification are needed [75,76].

Besides, those immunosensors that include nanostructures present a lack of control for the structuration and positioning of nano objects. Furthermore, the modulation of the electrical properties still challenging.

Herein, we overcome those problems with the present pioneering technique. Our technology involves the nano contact printing technique which integrate the low cost electrode fabrication in nonconductive materials and the efficient electro-immobilization of antibodies. The technology presented on this work is highly sensitive and easy to device. Successfully determination of cytokines can be performed at pg/mL concentrations and can reach LOD of sub ng/mL.

Furtheremore, several studies have documented high IL-6 levels in body fluids of patients with certain carcinomas. Typically, normal concentration of IL-6 in healthy individuals is less than 6 pg/mL, while mean serum IL-6 in patients is higher than 20 pg/mL [77]. The LOD and linear range of the present immunosensors permit to differentiate a healthy patient (Table 1).

4. Conclusions

We effectively fabricated PPyNWs using our pioneering printing technology on flexible thermoplastics (PEEK and PETE). PPy-NWs were characterized using AFM, SEM, XPS, CV, and EIS. Anti-human IL-6 monoclonal antibodies (mAb's, IL6) were chemically immobilized on a PPyNWs film using diazonium chemistry and cross linkers (carbodiimide). The successfully devised impedimetric immunosensors presented a sensitivity of 0.013 $(pg/mL)^{-1}$ and LOD of 0.36 pg/mL. The current technology can be applied for development of diagnostic tools and for biomarker determination.

Acknowledgements

To CONACYT (Mexican National Council of Science and Technology) Scholarship Program, the SMARTCANCERSENS project (FP7-PEOPLE-2012-IRSES) under the grant agreement No. 31805, the NATO project, SPS (NUKP.SFPP984173), the SEA-on-a-CHIP project (FP7-KBBE) (614168) and it reflects only the author's views.

Appendix A. Supplementary data

Supplementary data associated with this article can be found, in the online version, at http://dx.doi.org/10.1016/j.snb.2017.09.057.

References

[1] G. Zheng, F. Patolsky, Y. Cui, W.U. Wang, C.M. Lieber, Nat. Biotechnol. 23 (10) (2005) 1294–1301.
[2] S.K. Ray, A.K. Katiyar, A.K. Raychaudhuri, Nanotechnology 28 (9) (2017) 092001.
[3] X. Liu, X. Huo, P. Liu, Y. Tang, J. Xu, H. Ju, Biosens. Bioelectron. 92 (2017) 171–178.
[4] A. Zhang, G. Zheng, C.M. Lieber, Nanowire Field-Effect Transistor Sensors, in: Nanowires, Springer International Publishing, 2016, pp. 255–275.
[5] X. Sun, N. Hui, X. Luo, Microchim. Acta 184 (3) (2017) 889–896.
[6] S. Tripathy, S.R.K. Vanjari, V. Singh, S. Swaminathan, S.G. Singh, Biosens. Bioelectron. 90 (2017) 378–387.
[7] V. Kumar, P. Guleria, S.K. Mehta, Environ. Chem. Lett. (2017) 1–13.
[8] C. Zhan, G. Yu, Y. Lu, L. Wang, E. Wujcik, S. Wei, J. Mater. Chem. C 5 (7) (2017) 1569–1585.
[9] N. Aydemir, J. Malmström, J. Travas-Sejdic, Phys. Chem. Chem. Phys. 18 (12) (2016) 8264–8277.
[10] J.H. Kim, W.S. Chang, D. Kim, S.H. Cho, S.K. Seol, Mater. Chem. Phys. 147 (3) (2014) 1171–1174.
[11] M. Šetka, J. Drbohlavová, J. Hubálek, Sensors 17 (3) (2017) 562.
[12] T.L. Tran, T.X. Chu, D.C. Huynh, D.T. Pham, T.H.T. Luu, A.T. Mai, Appl. Surf. Sci. 314 (2014) 260–265.
[13] F. Xiao, L. Wang, H. Duan, Biotechnol. Adv. 34 (3) (2016) 234–249.
[14] Z.D. Kojabad, S.A. Shojaosadati, Mater. Des. 96 (2016) 378–384.
[15] D.J. Shirale, M.A. Bangar, M. Park, M.V. Yates, W. Chen, N.V. Myung, A. Mulchandani, Environ. Sci. Technol. 44 (23) (2010) 9030.
[16] J. Shan, Z. Ma, Microchim. Acta (2017) 1–11.
[17] J.M. Moon, Y.H. Kim, Y. Cho, Biosens. Bioelectron. 57 (2014) 157–161.
[18] D.V. Kalvakolanu, Cytokine 89 (2017) 1–3.
[19] T. Koga, K. Migita, S. Sato, M. Umeda, F. Nonaka, S.Y. Kawashiri, T. Origuchi, Medicine (Baltimore) 95 (16) (2016).
[20] D. Margel, M. Pevsner-Fischer, J. Baniel, O. Yossepowitch, I.R. Cohen, Eur. Urol. 59 (1) (2011) 113–119.
[21] S.O. Dima, C. Tanase, R. Albulescu, V. Herlea, M. Chivu-Economescu, R. Purnichescu-Purtan, T. Dumitrascu, D.G. Duda, I. Popescu, Pancreas 41 (7) (2012) 1001–1007.
[22] H. Sellami, N. Said-Sadier, A. Znazen, R. Gdoura, D.M. Ojcius, A. Hammami, Mol. Cell Probes 28 (4) (2014) 147–154.
[23] Y.J. Du, H.Y. Zhang, B. Li, X. Wu, Y.B. Lv, H.L. Jin, Y.X. Cao, J. Sun, Q.L. Luo, W.Y. Gong, B.J. Liu, J.F. Wu, S.X. Shi, J.C. Dong, Prog. Neuropsychopharmacol. Biol. Psychiatry 47 (2013) 6.
[24] M. Tahara, M. Schlumberger, R. Elisei, M.A. Habra, N. Kiyota, R. Paschke, T. Kadowaki, Eur. J. Cancer 75 (2017) 213–221.
[25] A. Abdel-Haq, B. Kusnierz-Cabala, D. Darczuk, E. Sobuta, P. Dumnicka, A. Wojas-Pelc, M. Chomyszyn-Gajewska, J. Periodontol. 85 (7) (2014) 956–965.
[26] C.H. Xu, P. Zhan, L.K. Yu, X.W. Zhang, Tumor Biol. 35 (2) (2014) 17.
[27] S.H. Faulkner, K.L. Spilsbury, J. Harvey, A. Jackson, J. Huang, M. Platt, A. Tok, M.A. Nimmo, Eur. J. Appl. Physiol. 114 (6) (2014) 1207–1216.
[28] Y. Liang, T. Ma, A. Thakur, H. Yu, L. Gao, P. Shi, X. Li, H. Ren, L. Jia, S. Zhang, Z. Li, M. Chen, Glycobiology 25 (3) (2015) 331–340.
[29] M.T. Lokant, R.K. Naz, Andrologia 47 (3) (2015) 328–332.
[30] U. Yogeswaran, S.M. Chen, Sensors 8 (1) (2008) 290–313.
[31] C. Cao, Y. Zhang, C. Jiang, M. Qi, G. Liu, ACS Appl. Mater. Interfaces 9 (6) (2017) 5031–5049.
[32] C. Jiang, S.M. Silva, S. Fan, Y. Wu, M.T. Alam, G. Liu, J. Gooding, J. Electroanal. Chem. 785 (2017) 265–278.
[33] M.M. Chehimi, Aryl Diazonium Salts: New Coupling Agents and Surface Science, John Wiley & Sons, 2012.
[34] M. Raicopol, A. Prună, C. Damian, L. Pilan, Nanoscale Res. Lett. 8 (1) (2013) 1–8.
[35] V. Mévellec, S. Roussel, L. Tessier, J. Chancolon, M. Mayne-L'Hermite, G. Deniau, P. Viel, S. Palacin, Chem. Mater. 19 (25) (2007) 6323–6330.
[36] J. Pinson, F. Podvorica, Chem. Soc. Rev. 34 (5) (2005) 429–439.
[37] M. Raicopol, C. Andronescu, R. Atasiei, A. Hanganu, L. Pilan, J. Electrochem. Soc. 161 (12) (2014) G103–113.
[38] S. Khetani, R. Aburashed, A. Singh, A. Sen, A. Sanati-Nezhad, Sens. Actuators B Chem. 247 (2017) 163–169.
[39] A. Hayat, L. Barthelmebs, A. Sassolas, J.L. Marty, Talanta 85 (1) (2011) 513–518.
[40] R. Wang, C. Xue, Anal. Methods 5 (19) (2013) 5195–5200.
[41] H. Qi, M. Li, R. Zhang, M. Dong, C. Ling, Anal. Chim. Acta 792 (2013) 28–34.
[42] G. Liu, S.G. Iyengar, J. Gooding, J. Electroanal. 24 (7) (2012) 1.
[43] R. Polsky, J.C. Harper, D.R. Wheeler, S.M. Dirk, D.C. Arango, S.M. Brozik, Biosens. Bioelectron. 235 (6) (2008) 757–764.
[44] G. Liu, J. Liu, T.P. Davis, J. Gooding, Biosens. Bioelectron. 265 (8) (2011) 3660–3665.
[45] R&D systems, USA., http://www.rndsystems.com/.
[46] M. Pino, N. Stingelin, K.E. Tanner, Acta Biomater. 4 (6) (2008) 1827–1836.
[47] H. Zhou, V.K. Goel, S.B. Bhaduri, Mater. Lett. 125 (2014) 96–98.
[48] A. Hadjizadeh, A. Ajji, M.N. Bureau, J. Mech. Behav. Biomed. 3 (8) (2010) 574–583.
[49] R. Ng, X. Zhang, N. Liu, S.T. Yang, Process Biochem. 44 (9) (2009) 992–998.
[50] G.P. Karayannidis, A.P. Chatziavgoustis, D.S. Achilias, Adv. Polym. Technol. 21 (4) (2002) 250–259.
[51] A. Garcia-Cruz, N. Zine, M. Sigaud, M. Lee, P. Marote, P. Lanteri, J. Bausells, A. Errachid, Microelectron. Eng. 121 (2014) 167–174.
[52] A. Baraket, N. Zinean, M. Lee, J. Bausells, N. Jaffrezic-Renault, F. Bessueille, N. Yaakoubi, A. Errachid, Microelectron. Eng. 111 (2013) 332–338.
[53] M. Lee, M.J. Lopez-Martinez, A. Baraket, N. Zine, J. Esteve, J.A. Plaza, N. Jaffrezic-Renault, A.J. Errachid, Polym. Sci. Part A: Polym. Chem. 51 (1) (2013) 59–70.
[54] G. Hammouri, A. Dana, B. Sunar, Cryptographic Hardware and Embedded Systems - CHES Ed. Christophe Clavier and Kris Gaj, Lecture Notes in Computer Science 5747, Springer Berlin Heidelberg, 2009, pp. 348–362.
[55] GeSiM (2011). http://www.gesim.de/en/contact-printers/procedure/.
[56] R. Mukherjee, R.C. Pangule, A. Sharma, I. Banerjee, J. Chem. Phys. 127 (2007) 064703.
[57] Viswanathan Meenakshi, Babayan Yelizaveta, W.J. Odom Teri, Chem. Educ. 84 (2007) 1795.
[58] D. Chowdhury, A. Paul, A. Chattopadhyay, Nano Lett. 1 (8) (2001) 409.
[59] D. Bello-Gil, B. Maestro, J. Fonseca, J.M. Feliu, V. Climent, J.M.S.M. Wanunu, PLoS One 9 (1) (2014).
[60] Y. Qiao, L. Shen, Y. Guo, Mater. Lett. 86 (1) (2012) 38–41.
[61] E. Gonzalez, M.D. Barankin, P.C. Guschl, R.F. Hicks, Langmuir 24 (21) (2008) 12636–12643.
[62] Y. Qiao, L. Shen, Y. Guo, Mater. Lett. 86 (2012) 38–41.
[63] S. Zhang, F. Awaja, N. James, D.R. McKenzie, A. Ruys, J. Colloids Surf. A 374 (1) (2011) 88–95.
[64] S. Zhang, F. Awaja, N. James, D.R. McKenzie, A. Ruys, J. Polym. Adv. Technol. 22 (12) (2011) 2496–2502.
[65] F. Awaja, S. Zhang, N. James, D.R. McKenzie, Plasma Processes Polym. 7 (9-10) (2010) 866–875.
[66] Yongsheng Qiao, Lazhen Shen, Yong Guo, Mater. Lett. 86 (2012) 38–41.
[67] J.E.B. Randles, Disc. Faraday Soc. 1 (0) (1947) 11–19.
[68] B.P. Corgier, C.A. Marquette, L.J. Blum, J. Am. Chem. Soc. 127 (51) (2005) 18328–18332.
[69] A. Baraket, M. Lee, N. Zine, M. Sigaud, N. Yaakoubi, M.G. Trivella, M. Zabala, J. Bausells, N. Jaffrezic-Renault, A. Errachid, Sens. Actuators B 189 (2013) 165–172.
[70] B.P. Corgier, A. Laurent, P. Perriat, L.J. Blum, C.A. Marquette, Angew. Chem. Int. Ed. 46 (22) (2007) 4108–4410.
[71] C. Combellas, F. Kanoufi, D. Mazouzi, A. Thiébault, P. Bertrand, N. Médard, Polymer 44 (1) (2003) 19–24.
[72] P.A. Brooksby, A.J. Downard, Langmuir 20 (2) (2004) 5038–5045.
[73] F. Anariba, S.H. DuVall, R.L. McCreery, Anal. Chem. 75 (15) (2003) 3837–3844.
[74] I. Vancurova, Cytokine Bioassays-Methods Protocols 1172 (2014) 49–64.
[75] B.S. Munge, T. Stracensky, K. Gamez, D. Dibiase, Electroanalysis 28 (2016) 2644–2658.
[76] B.V. Chikkaveeraiah, A.A. Bhirde, N.Y. Morgan, H.S. Eden, X. Chen, ACS Nano 8 (2012) 6546–6561.
[77] R. Laocharoensuk, Electroanalysis 28 (2016) 1716–1729.
[78] T. Yang, S. Wang, H. Jin, W. Bao, S. Huang, J. Wang, Sens. Actuators B Chem. 178 (2013) 310–315.
[79] R. Malhotra, V. Patel, B.V. Chikkaveeraiah, B.S. Munge, C. Cheong, R.B. Zain, M.T. Abraham, D.K. Dey, J.S. Gutkind, Anal. Chem. 84 (14) (2013) 6249–6255.

[80] L.S.S. Kumar, X. Wang, J. Hagen, R. Naik, I. Papautsky, J. Heikenfeld, Anal. Methods 20 (2016) 1–5.
[81] Z. Yang, M. Lu, J. Li, Z. Tan, H. Dai, X. Jiao, X. Hu, Biosens. Bioelectron. 89 (2017) 558–564.
[82] M. Braiek, Y. Yang, C. Farre, C. Chaix, Bessueille Electroanal. 28 (2016) 1810–1816.
[83] C.E. Krause, B.A. Otieno, G.W. Bishop, G. Phadke, L. Choquette, R.V. Lalla, D.E. Peterson, J.F. Rusling, Anal. Bioanal. Chem. 407 (2015) 7239–7243.
[84] Y. Lou, T. He, F. Jiang, J. Shi, J. Zhu, Talanta 122 (2014) 135–139.
[85] J. Peng, J. Peng, L. Feng, Z. Ren, L. Jiang, J. Zhu, Small 7 (20) (2011) 2921–2928.
[86] M. Lee, N. Zine, A. Baraket, M. Zabala, F. Campabadal, R. Caruso, M.G. Trivella, N. Jaffrezic-Renault, A. Errachid, Sens. Actuators B Chem. 175 (2012) 201–207.
[87] G. Wang, X. He, L. Chen, Y. Zhu, X. Zhang, Colloids Surf. B Biointerfaces 116 (2014) 714–719.
[88] E. Sanchez-Tirado, C. Salvo, A. Gonzalez-Cortes, P. Yanez-Sedeno, F. Langa, J.M. Pingarron, Anal. Chim. Acta 959 (2017) 66–73.
[89] G. Fan, X. Ren, C. Zhu, J. Zhang, J. Zhu, Biosens. Bioelectron. 59 (2014) 45–53.
[90] I. Ojeda, M. Moreno-Guzmán, A. Gonzalez-Cortes, P. Yanez-Sedeno, J.M. Pingarron, Anal. Bioanal. Chem. 406 (2014) 6363–6371.
[91] G.A. Messina, N.V. Panini, N.A. Martinez, J. Raba, Anal. Biochem. 380 (2008) 262–267.
[92] T. Li, M. Yang, Sens. Actuators B Chem. 158 (1) (2011) 361–365.
[93] G. Wang, H. Huang, G. Zhang, X. Zhang, B. Fang, L. Wang, Langmuir 27 (25) (2011) 1224–1231.
[94] H. Chen, T. Kian, J. Huang, Y. Wang, Y. Liu, M. Platt, A. Palaniappan, B. Liedberg, A. Iing, Y. Tok, Mater. Des. 90 (2016) 852–857.
[95] C. Deng, F. Qu, H. Sun, M. Yang, Sens. Actuators B Chem. 160 (1) (2011) 471–474.
[96] J.T. Belle, K. La Demirok, R. Patel, C.B. Cook, Analyst 136 (2011) 1496–1501.
[97] Jingfeng Huang, James Harvey, W.H. Derrick Fam, Myra A. Nimmo, I.Y. Alfred Tok, Novel biosensor for Interleukin-6 detection, Procedia Eng. 60 (2013) 195–200.
[98] G.C. Jensen, C.E. Krause, A. Sotzing, J.F. Rusling, Phys. Chem. Chem. Phys. 13 (2011) 4888–4894.
[99] S. Campuzano, V.R. Montiel, M. Gamella, Biosens. Bioelectron. 77 (2016) 543–548.
[100] R. Sharma, S.E. Deacon, D. Nowak, S.E. George, M.P. Szymonik, A.A.S. Tang, D.C. Tomlinson, A.G. Davies, M.J. Mcpherson, C. Wälti, Biosens. Bioelectron. 80 (2016) 607–613.
[101] K. Zhong, W. Jun, Anal. Chim. Acta 580 (2006) 128–135.
[102] M. Lee, N. Zine, A. Baraket, M. Zabala, F. Campabadal, R. Caruso, M. Giovanna, N. Jaffrezic-renault, A. Errachid, Sens. Actuators B Chem. 175 (2012) 201–207.
[103] A. Baraket, M. Lee, N. Zine, M.G. Trivella, M. Zabala, J.A. Bausells, Procedia Eng. 87 (2014) 377–379.

Biographies

Alvaro Garcia Cruz received his BSc (Hons) in Chemistry from the University of Guanajuato (Mexico) and his master degree (Hons) in Catalysis and Physical Chemistry at the University Claude Bernard Lyon 1 (France) in 2010. He completed his Ph.D. studies at the University Claude Bernard Lyon 1 (France) under the supervision of Prof. Abdelhamid Errachid and Prof. Monique Sigaud in Nano and Biotechnology under the scholarship excellence program sponsored by the National Council of Science and Technology (CONACYT) from 2012 to 2015. He worked as assistant professor in the Institute of Physical Chemistry of the Polish Academy of Science in Warsaw (Poland) in the group of Prof. W. Kutner from 2015 to 2017. Currently he is working at the University of Leicester (UK) in the group of Prof Sergey A. Piletsky on chemosensors based on molecularly imprinted polymers (MIPs). His research interest focuses on electrochemical sensors, bioelectronics, paper based sensors, gas sensors, microfabrication and microfluidics, bio-functionalization and nano-biotechnology.

Faiza NESSARK obtained her engineer degree in 2003 and in 2006 her master degree in electrochemical engineering from the University of Ferhat Abbas Setif 1, Algeria. In 2014, she was visiting researcher at the Institute of Analytical Sciences (ISA), Lyon, France. She obtained her PhD in 2017 under supervision of Prof. Errachid. Since 2010 she is assistant researcher in Laboratory of Electrochemistry and Materials at the Faculty of Technology, University of Ferhat Abbas Setif 1. She is working also as lecturer at the University of M'Sila, Algeria. Her research interest focuses on the development and characterization of composites and new materials modified with polypyrrole films for electrocatalysis.

Michael Lee received his BSc (Hons) in Forensic Science from Northumbria University, Newcastle (UK) in 2004 and his MSc (Hons) in Analytical Chemistry from Teesside University, Middlesbrough (UK) in 2006. In 2013, he completed his Ph.D. in Analytical Chemistry and Bioengineering at the Université de Lyon1 (Lyon, France) in the group of Prof. Errachid. Between 2014–2015, he continued as a postdoctoral research to develop a functionalized Lab-on-Chip unit. From 2015 to 2016, he joined the group of Prof. Robert S. Marks at Nanyang Technological University (Singapore) as a postdoctoral research fellow. He has a research background in bioengineering and nanotechnology and most recently as a scientific grant writer.

Nadia Zine was graduated in Chemistry from the University M. Ismail, Meknes, in 1994. She received a Master in Material Science in 1997 and a PhD degree in Chemistry in 2005, both from the Universitat Autonoma de Barcelona, Spain. From 2006 to 2009 she worked in the Barcelona Scientific Park within the Spanish Juan de la Cierva Program.From 2010, she became a lecturer at the UCBL. She's author and co-author of 45 papers and more than 68 communications in scientific meetings. Her research interest is the electrochemical Characterization of Chemical Sensors and Biosensors, Especially of ISFET devices and microelectrodes.

Monique Sigaud was born Baret on 1969/12/10 in Bourgoin-Jallieu (France). She received his BSc in chemistry from the Joseph Fourier University of Grenoble (France) and his Ph. D. in Ion Selective Electrodes and Chemometrics at the Vrije Universiteit Brussel (Belgium). Monique Sigaud was lecturer at the Ecole Nationale Supérieure d'Electrochimie et d'Electrométallurgie de Grenoble (INP Grenoble) from 2000 to 2003. She is researcher at Institute of Analytical Sciences (Lyon) since 2003 and head of the Chemistry Department of IUT Lyon1 since 2016.

R. Pruna graduated in Physics (Universitat de Barcelona, 2014), and is MSc. in Biomedical Engineering (Universitat de Barcelona and Universitat Politècnica de Catalunya, 2016). Currently she is a Ph.D. student at the Universitat de Barcelona, and her research is focused on new nanostructured transducers for electrochemical biosensors.

Manel López, PhD (2000) is associate professor at the University of Barcelona (UB). His research is basically focused in the field of sensor networks, working from the development of the sensor itself to the design of the whole network. Nowadays he is working in the instrumentation needed to supply and acquire the signals from the sensors.

Pedro Marote recived his BSc in Chemistry 1996 from University Claude Bernard Lyon 1(France). In 1996 he worked as researcher in the Laboratory of Energy and Inorganic Synthesis. In 2001 he received his Ph.D. in Chemistry. He worked at the Laboratory of Analytical Sciences from 2002 to 2011. Since 2006 he works as engineer in the Institute of Analytical Sciences. Their research interest focus on Formulation topics and surface analysis (MEB).

Joan Bausells received the Ph.D. degree in Physics from the University of Barcelona, Spain, in 1986. From 1981 to 1986, he was an R&D Engineer in the semiconductor industry. In 1986 he joined IMB-CNM, where he has been a permanent researcher since 1988, and a Research Professor since 2002. At IMB-CNM, he has been a Manager of the Sensors and Actuators Group (1990–1996), the Microsystems Department (1999–2002), the Nanotechnology Group (2002–2006), and has been Vicedirector (2008–2012) and Acting Director (2012). His early work was on theory of condensed matter and in microelectronics technology. His research activities in the microsystems field include contributions to micromachining technology, CMOS, sensors, MEMS design kits and (bio)chemical sensors. He has managed 11 projects of the Research Framework Programmes of the European Union and has coordinated two of them. He is the coauthor of more than 100 journal papers and 230 conference presentations.His current research interests include micro- and nanoelectromechanical structures and nanoelectronic devices, and their applications to micro/nano (sensor) systems.

Nicole Jaffrezic-Renault received her engineering degree from the Ecole Nationale Supérieure de Chimie, Paris, in 1971 and the Doctorat d'Etat és Sciences Physiques from the University of Paris in 1976. She joined Ecole Centrale de Lyon, France in 1984 and Claude Bernard University Lyon 1 in 2007. As Director of Research at the Centre National de la Recherche Scientifique, past President of the Chemical Micro Sensor Club (CMC2), President of the Analytical Division of the French Chemical Society, her research activities in the Institute of Analytical Sciences, include conception and design of (bio)chemical sensors and their integration in microsystems. She is President of the Analytical Chemistry Division of the Chemical Society of France. She coordinates several European and national projects for the development of microsystems for biomedical and environmental monitoring and for food safety. She published more than 500 papers with more than 7900 citations.

Prof. Abdelhamid Errachid received his Ph.D degree from the Universitat Autonoma de Barcelona in 1997. From 1997 until 2001 he worked as junior research scientist at the CNM. From 2001 till 2008 he worked as senior research at the department de electronica, Universidad de Barcelona and IBEC. Finally, since the end of 2008, he is a full professor at the University Claude Bernard-Lyon 1. He has been involved as a coordinator, principal investigator, and team leader in several European projects under 5th, 6th, 7th and H2020 framework programmes: FP6: (DVT-IMP, MAPTech, SPOT-NOSED, Nano2Life, Ares, Vector), FP7 (SensorART, BOND and H2020 (HEARTEN), as well as NATO, INTAS and TEMPUS International projects and national Spanish projects (MIROMINCE, MINAHE, I, MINAHE II and PETRI). Prof. Errachid was a head of the SIMS (Surfaces- (bio) Interface- Micro/nano Systèmes) group from 2009 until 2013 and now he is a head of the micro&nanobiotechnology group.